



UNIVERSITY OF LEEDS

This is a repository copy of *Co-populated Conformational Ensembles of  $\beta(2)$ -Microglobulin Uncovered Quantitatively by Electrospray Ionization Mass Spectrometry* .

White Rose Research Online URL for this paper:  
<http://eprints.whiterose.ac.uk/608/>

---

**Article:**

Borysik, A.J.H., Radford, S.E. and Ashcroft, A.E. (2004) Co-populated Conformational Ensembles of  $\beta(2)$ -Microglobulin Uncovered Quantitatively by Electrospray Ionization Mass Spectrometry. *Journal of Biological Chemistry*, 279 (26). pp. 27069-27077. ISSN 1083-351X

<https://doi.org/10.1074/jbc.M401472200>

---

**Reuse**

See Attached

**Takedown**

If you consider content in White Rose Research Online to be in breach of UK law, please notify us by emailing [eprints@whiterose.ac.uk](mailto:eprints@whiterose.ac.uk) including the URL of the record and the reason for the withdrawal request.



[eprints@whiterose.ac.uk](mailto:eprints@whiterose.ac.uk)  
<https://eprints.whiterose.ac.uk/>

# Co-populated Conformational Ensembles of $\beta_2$ -Microglobulin Uncovered Quantitatively by Electrospray Ionization Mass Spectrometry\*<sup>§</sup>

Received for publication, February 10, 2004, and in revised form, March 31, 2004  
Published, JBC Papers in Press, April 20, 2004, DOI 10.1074/jbc.M401472200

Antoni J. H. Borysik, Sheena E. Radford<sup>‡</sup>, and Alison E. Ashcroft<sup>§</sup>

From the Astbury Centre for Structural Molecular Biology, School of Biochemistry and Microbiology, University of Leeds, Leeds LS2 9JT, United Kingdom

**Ordered assembly of monomeric human  $\beta_2$ -microglobulin ( $\beta_2$ m) into amyloid fibrils is associated with the disorder hemodialysis-related amyloidosis. Previously, we have shown that under acidic conditions (pH <5.0 at 37 °C), wild-type  $\beta_2$ m assembles spontaneously into fibrils with different morphologies. Under these conditions,  $\beta_2$ m populates a number of different conformational states *in vitro*. However, this equilibrium mixture of conformationally different species is difficult to resolve using ensemble techniques such as nuclear magnetic resonance or circular dichroism. Here we use electrospray ionization mass spectrometry to resolve different species of  $\beta_2$ m populated between pH 6.0 and 2.0. We show that by linear deconvolution of the charge state distributions, the extent to which each conformational ensemble is populated throughout the pH range can be determined and quantified. Thus, at pH 3.6, conditions under which short fibrils are produced, the conformational ensemble is dominated by a charge state distribution centered on the 9+ ions. By contrast, under more acidic conditions (pH 2.6), where long straight fibrils are formed, the charge state distribution is dominated by the 10+ and 11+ ions. The data are reinforced by investigations on two variants of  $\beta_2$ m (V9A and F30A) that have reduced stability to pH denaturation and show changes in the pH dependence of the charge state distribution that correlate with the decrease in stability measured by tryptophan fluorescence. The data highlight the potential of electrospray ionization mass spectrometry to resolve and quantify complex mixtures of different conformational species, one or more of which may be important in the formation of amyloid.**

$\beta_2$ -microglobulin ( $\beta_2$ m)<sup>1</sup> is one of a number of proteins known to aggregate into insoluble amyloid deposits *in vivo* (1–3). These amyloid deposits have been linked to various human

maladies such as Alzheimer's disease (4), Huntington's chorea (5), and senile systemic amyloidosis (6). However, for the majority of the ~20 known amyloid-related proteins, the structural mechanism of amyloid formation is still unclear, and, for several proteins, the role that different aggregated states play in the manifestation of the disease symptoms remains unresolved (7).

$\beta_2$ m is a small (11,860-dalton) extracellular protein that forms the nonpolymorphic light chain component of the major histocompatibility class I complex. The physiological role of  $\beta_2$ m has been likened to a chaperone in that it is required for the heavy chain of the major histocompatibility class I complex to fold into a stable secreted entity (8, 9).  $\beta_2$ m is an all  $\beta$ -sheet protein, with a seven-stranded  $\beta$ -sandwich structure and a single disulfide bond linking Cys-25 and Cys-80 in the B and F strands (10) (Fig. 1). In healthy individuals, the serum concentration of circulating free  $\beta_2$ m is ~3 mg·liter<sup>-1</sup> (11), and the protein is removed from the serum by renal catabolism (12). In individuals undergoing renal dialysis, the serum concentration of  $\beta_2$ m can rise to around 50 times the levels in healthy individuals (13, 14). In these patients, the deposition of predominantly full-length wild-type  $\beta_2$ m into amyloid fibrils is inevitable, with all patients who undergo long term hemodialysis eventually developing the systemic condition, dialysis-related amyloidosis (13).

Partial unfolding of monomeric  $\beta_2$ m has been shown to be required *in vitro* for fibrillogenesis to proceed on an experimentally tractable time scale. This can be accomplished by acidification of the solution (15), truncation of six amino acids from the N terminus (16), or the addition of Cu<sup>2+</sup> ions (17). Depending on the denaturing conditions used, a number of different fibril morphologies are formed *in vitro* (18, 19). For example, short curved fibrils (~200 nm) are formed at pH ~3.6 at high ionic strength (0.4 M), whereas under more acidic conditions (pH ~2.5) and low ionic strength ( $\leq$ 50 mM), longer (~1  $\mu$ m) and straighter amyloid-like fibrils are formed. Both fibril types give rise to x-ray fiber diffraction patterns typical of a cross- $\beta$  structure and bind the histopathological dyes thioflavin-T and Congo red (20).

At pH ~3.6,  $\beta_2$ m adopts a partially folded state, as indicated by a number of techniques including CD and the fluorescence of 1-anilinonaphthalene-8-sulfonic acid (15). This species is also weakly protected from hydrogen exchange and gives rise to broad resonances in NMR spectra (21). Thus, it displays the hallmarks of a partially folded or molten globule state. At more acidic pH (pH 2.5), monomeric  $\beta_2$ m is also weakly protected from hydrogen exchange, and, although it retains some residual structure, it is largely disordered, as determined by NMR (22). It has been suggested that the observed differences in the fibril morphologies formed from  $\beta_2$ m at pH 3.6 and pH 2.5 could

\* This work was supported by the University of Leeds, the Wellcome Trust, the Biotechnology and Biological Sciences Research Council (BBRSC), and Micromass UK Ltd./Waters Ltd. The costs of publication of this article were defrayed in part by the payment of page charges. This article must therefore be hereby marked "advertisement" in accordance with 18 U.S.C. Section 1734 solely to indicate this fact.

<sup>§</sup> The on-line version of this article (available at <http://www.jbc.org>) contains one additional figure.

<sup>‡</sup> A BBRSC Professorial Fellow.

<sup>§</sup> To whom correspondence should be addressed: Astbury Centre for Structural Molecular Biology, School of Biochemistry & Microbiology, University of Leeds, Leeds LS2 9JT, United Kingdom. Tel./Fax: 44-113-3437273; E-mail: a.e.ashcroft@leeds.ac.uk.

<sup>1</sup> The abbreviations used are:  $\beta_2$ m,  $\beta_2$ -microglobulin; BPI, base peak intensity; ESI, electrospray ionization; MS, mass spectrometry; EM, electron microscopy.

reflect the different conformational states of the monomeric protein under each condition, although other models, including a kinetic rather than a structural dependence of fibril morphology on pH, are also consistent with the current experimental data (18, 21). A major problem in identifying which of these models is correct is that quantification of the relative concentrations of native, partially folded, and acid-unfolded states, which may be co-populated under conditions in which the protein is fibrillogenic, cannot be obtained using spectroscopic methods. This is because these techniques provide only the population-weight average property under each condition. Electrospray ionization mass spectrometry (ESI-MS), however, has the unique capability of resolving multiple species that are co-populated in solution, provided that these species give rise to different charge state distributions (23–26). Several models have been proposed to rationalize the observed differences in the charge state distributions of native and nonnative states. Differences in the solvent accessibility of ionizable groups (23, 27), heightened Coulomb energies of folded compared with unfolded polyprotonated conformations (28, 29), or the increased protection against charge neutralization offered by native protein conformations (30) have all been offered as plausible explanations. Whichever mechanism or combination of processes governs this phenomenon, the net result is that conformational species with more open structures carry, on average, more charges and produce broader ion envelopes centered on higher charge states than their more compact native counterparts (31).

Here we describe the use of ESI-MS, combined with quantitative analysis of the charge state distributions generated, to investigate the population of native, partially folded, and acid-unfolded conformers of  $\beta_2m$  as a function of pH. Using this approach, we show that the population of different species can be quantified using ESI-MS and compared with denaturation of the protein followed by intrinsic tryptophan fluorescence. The data are reinforced by similar analyses of two destabilized  $\beta_2m$  mutants, V9A and F30A (20, 32) (Fig. 1). These proteins adopt native-like structures at neutral pH but are significantly destabilized at lower pH. Thus, the pH at which the partially folded state first becomes significantly (>5%) populated (named herein as the N-I transition point) occurs at pH 4.8, 5.6, and 5.3 for wild-type, V9A, and F30A  $\beta_2m$ , respectively. Similarly, titration with urea results in midpoints of 4.7, 1.6, and 2.9 M urea for wild-type, V9A, and F30A  $\beta_2m$ , respectively (20, 32). Importantly, and by contrast with wild-type and F30A  $\beta_2m$ , V9A forms amyloid-like fibrils at neutral pH (*i.e.* under conditions where the protein is natively folded) (32). Both variants were carefully selected from a series of mutants previously constructed as part of a systematic study on the role of global stability in  $\beta_2m$  fibrillogenesis (20, 32) on the premise that they should possess pH stabilities significantly different from that of wild-type  $\beta_2m$ , without dramatic perturbation of their overall gas phase proton affinities or the upper limit of charges attainable. Thus, they provide ideal controls for systematic deconvolution of the charge state distribution as a function of pH.

#### EXPERIMENTAL PROCEDURES

**Reagents**—All reagents were purchased from Sigma. To minimize contamination from salts, buffers were prepared in water suitable for trace inorganic analysis (Fluka, Gillingham, Dorset, UK) and acidified with volumetric standard HCl, 1.0 N (Sigma).

**Buffers**—Careful consideration of the buffering system used was required in order to optimize the spread of the charge state distribution of  $\beta_2m$  and hence the resolution of the different protein conformers while maintaining ESI-MS-compatible conditions. Thus, all ESI-MS experiments were carried out in a composite buffer containing 5 mM ammonium formate and 5 mM ammonium acetate. HCl rather than a volatile organic acid was used to adjust the pH to the desired value throughout the pH range, because this was found to generate the widest

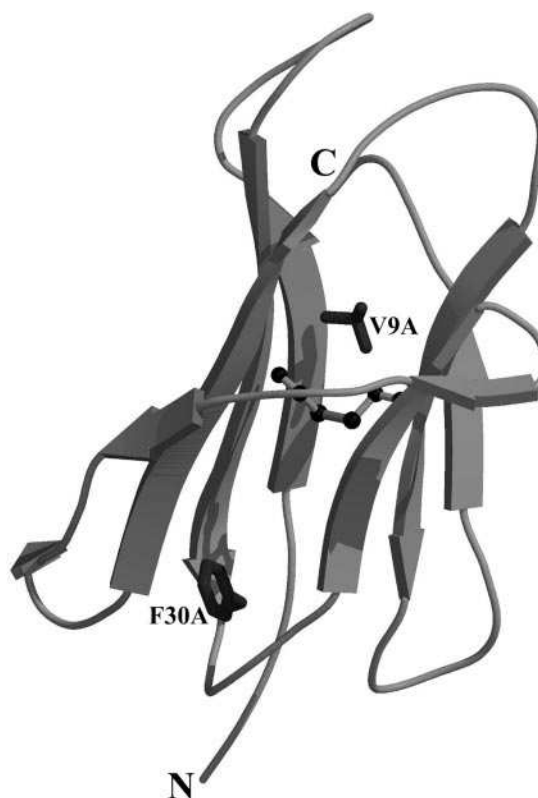


FIG. 1. Ribbon diagram of human  $\beta_2m$  taken from the crystal structure of the protein bound to the heavy chain of the major histocompatibility class I complex (Protein Data Bank number 1DUZ) (46). Residues Val-9 and Phe-30, which were changed to alanine in the mutants V9A and F30A, and the disulfide bond are shown as *ball and stick*. The figure was drawn using MOLSCRIPT (47).

charge state distribution of  $\beta_2m$  under the denaturing conditions used. In addition, salt concentrations of >10 mM were avoided, since the number of observed charge states decreased at higher ionic strengths, resulting in the loss of the high  $m/z$  ions. Fluorescence experiments and fibril growth experiments were also conducted using this buffer system as well as a higher ionic strength buffer containing 25 mM ammonium formate and 25 mM ammonium acetate. The two buffer systems are referred to as “low salt” (5 mM ammonium formate and 5 mM ammonium acetate) and “high salt” (25 mM ammonium formate and 25 mM ammonium acetate) throughout.

**ESI-MS**—All experiments were performed on a Platform II ESI-MS mass spectrometer (Micromass UK Ltd./Waters Ltd. (Manchester, UK)) operated under MassLynx software control. The source temperature was maintained at 37 °C with capillary and cone voltages of 3.5 kV and 50 V, respectively. Samples were infused using a syringe pump (Harvard Apparatus, Holliston, MA) at a flow rate of 20  $\mu\text{L}\cdot\text{min}^{-1}$ . Recombinant  $\beta_2m$  was overexpressed and purified as described previously (18). Protein was dissolved in Purite deionized water (Purite Analyst HP 25, Purite Ltd., Thame, Oxfordshire, UK) at a concentration of 200  $\mu\text{M}$ , syringe-filtered (0.2  $\mu\text{m}$ ) to remove any potential preaggregated states (18), and dialyzed extensively overnight in a 3500 molecular weight cut-off Slide-a-lyser (Pierce) with 5 liters of Purite water at 4 °C. Next, samples were diluted 1:10 (v/v) with the appropriate buffer and then equilibrated at 37 °C for ~30 min before injection. No significant differences were observed in the charge state distributions of samples infused after an incubation for several hours with the instrumental conditions used. The capillary was pre-equilibrated with 100  $\mu\text{L}$  of buffer at the appropriate pH prior to sample injection. Ten 10-s spectra were acquired in multichannel analysis mode for each sample. Instrument calibration was achieved with a separate introduction of horse heart myoglobin to ensure a mass accuracy to within  $\pm 0.01\%$ .

**Deconvolution of ESI-MS Spectra**—All the  $m/z$  spectra were processed using a two-point smooth with a Savitsky-Golay algorithm (supplied with the MassLynx software) using a measured 1.0-dalton peak width at half height. These smoothed  $m/z$  spectra are shown in Fig. A in the Supplementary Material. Next, each of these spectra was subjected to a centroiding process, which created a centroided (or “stick”) spec-

trum by measuring the peak area of the top 90% of each peak in the spectrum. Each spectrum showed evidence for the protein primarily as protonated molecular ions with a varying number of charges (*i.e.*  $m/z = (M + n_H^{n^+})/n$ ). There were also minor signals originating from salt adducts, in particular potassium. In order to account for this, the total ion current between each protonated molecular ion charge state and its corresponding dipotassium adduct ions were summed together (Fig. Aii in Supplementary Material). These new values were normalized to the base peak intensity and expressed in terms of percentage of base peak intensities (BPI). This procedure resulted in a significant improvement in the agreement between the ion currents of observed quasimolecular ions with replicate analysis. This process assumes equivalence in the capacity of different protein conformers to acquire these adducts. To fit the resulting spectra to a series of gaussian distributions, a method similar to that of Dobo and Kaltashov was used (33). This method assumes that the total ion current in any given ESI-MS spectrum can be described by a linear combination of a limited number of gaussian functions, each one arising from a different conformational ensemble of the protein at equilibrium.

Each charge state was plotted in ASCII-XY format against its recalculated percentage of BPI (above), and the S.D., mean, and amplitude of a limited number of gaussian distributions were allowed to vary freely using PeakSolve (Thermo Electron Corp., Altrincham, UK) so that the residual error between the combined linear contribution of these gaussian functions and the experimental data was minimized. Any remaining error between the experimental data and the gaussian functions was reduced using least squares regression using Solver (Microsoft Corp.) to minimize the squared error between the sum of the gaussian amplitudes at each charge state and the corresponding charge state percentage of BPI by subtle adjustment of the S.D., mean, and amplitude of each gaussian function.

The precision of each local fit was continually assessed globally during the deconvolution process. This was necessary because of the limited number of experimental observations arising from this technique (single integer values from the charge states 5+ to 15+) as well as the restricted resolution between the charge state distributions of the partially folded and acid-unfolded states of  $\beta_2m$ , which, in some instances, resulted in more than one possible local minimized fit when both of these populations were present. The fitting process assumed that the envelope of peaks observed in each ESI-MS spectrum is made up of several ion abundance patterns  $I_{(z)}$ , each one representing one or more different protein conformers coexisting at equilibrium, and it is possible to explain each of these by normalized gaussian distribution functions,

$$I_{(z)} = \frac{1}{\sigma \sqrt{2\pi}} e^{-1/2 \left( \frac{\chi - \mu}{\sigma} \right)^2} \quad (\text{Eq. 1})$$

where  $\mu$  and  $\sigma$  represent the mean and the S.D. of the distribution of charges of each of the protein conformers. These values were assumed not to vary significantly for each population throughout the pH titration. By contrast, the relative intensity (amplitude) of each function will vary depending on the extent to which each conformational ensemble is populated at each pH. Furthermore, a relationship was assumed to exist between the width of the charge state distribution (*i.e.* the gaussian standard deviation of each ion abundance pattern) and each conformational state, such that  $\sigma$  increases in the order native < partially folded < acid-unfolded. Then the population of each conformer was calculated by summation of the height,  $I_{(z)}$ , of every integer value (charge state) under each gaussian function found in each spectrum. Finally, these values were normalized as a percentage contribution of each conformer to the total ion current.

**Acid Denaturation of  $\beta_2m$  Followed by Tryptophan Fluorescence**—Fluorescence experiments were performed on a C-61 spectrofluorimeter (Photon Technology International Inc., Ford, West Sussex, UK) with excitation and emission wavelengths of 280 and 327 nm, respectively. Lyophilized protein samples were dissolved in Purite water, filtered (0.2  $\mu\text{M}$ ), and then diluted into Purite water to a final protein concentration of 40  $\mu\text{M}$ . Samples were then diluted 1:10 (v/v) into the appropriate low salt buffer and allowed to equilibrate in a 10-mm quartz cuvette (Hellma UK Ltd., Southend on Sea, Essex, UK) contained in a heated Peltier unit at 37 °C for 6 min prior to data acquisition. Under these conditions, the fluorescence signal was constant over the acquisition time. Further, both wild-type and F30A  $\beta_2m$  showed no time-dependent signal changes over the total incubation time under these conditions. Fluorescence intensities were measured between pH 6.2 and 2.0 for 60 s and averaged for each sample; then each denaturation curve was normalized to its fluorescence intensity at pH 6.2.

**Comparison of Acid Denaturation Monitored by Fluorescence and ESI-MS**—To compare the pH denaturation profiles of  $\beta_2m$  measured by ESI-MS and fluorescence, the fluorescence emission of the protein at 327 nm ( $\lambda$  excitation 280 nm) was measured as a function of pH and compared with data computed directly from the known relative populations of native, partially folded, and acid-unfolded  $\beta_2m$  determined by ESI-MS. This process assumes that each conformer has a different fluorescence intensity at pH 6.0 and that each signal varies linearly with pH. In addition, when comparing wild-type and F30A  $\beta_2m$ , it was assumed that the fluorescence intensities of the partially folded and acid-unfolded states are identical in the two proteins, although the fluorescence signal of the native state of F30A is greater than that of wild-type  $\beta_2m$  (>5% increase in fluorescence signal intensity at pH 6.0) (20).

The fluorescence value at each pH was calculated according to Equation 2,

$$F_c = ([N] \cdot Fl_N) + ([I] \cdot Fl_I) + ([A] \cdot Fl_A) \quad (\text{Eq. 2})$$

where [N], [I], and [A] correspond to the relative populations of native, partially folded, and acid-unfolded species at each pH value determined from deconvolution of the ESI-MS  $m/z$  spectra, and  $Fl_N$ ,  $Fl_I$ , and  $Fl_A$  represent the fluorescence signals of these states at each pH value. The pH dependence of the fluorescence signal of the partially folded and acid-unfolded conformations was allowed to vary in order to achieve the best fit. Since it was possible to measure directly the fluorescence intensity of the native state of wild-type  $\beta_2m$  and F30A  $\beta_2m$  over the pH ranges of 6.2 to 5.0 and 6.2 to 5.6, respectively, the pH dependence of the fluorescence signal of this state was determined experimentally for these proteins and held as a constant throughout the fitting procedure. The fluorescence signals for the partially folded and acid-unfolded states were 0.57 and 0.80 at pH 6.0 (normalized to the fluorescence intensity of the native state at pH 6.2) with pH dependences of 0.05 and 0.08 units per pH value, respectively. The native state fluorescence signals at pH 6.0 were 0.99 and 0.98 for wild-type and F30A  $\beta_2m$ , respectively, with corresponding pH dependences of 0.06 and 0.01 units per pH value. The fitting process was carried out using least squares regression between the experimentally derived equilibrium denaturation data and  $F_c$ , which was achieved using Solver (Microsoft).

**Fibril Formation from Wild-type  $\beta_2m$** —Recombinant wild-type  $\beta_2m$  was dissolved in Purite water, syringe-filtered (0.2  $\mu\text{m}$ ), and then dissolved 1:10 (v/v) into the appropriate buffer to give a final protein concentration of 0.2  $\text{mg} \cdot \text{ml}^{-1}$ . A 0.75-ml aliquot of each solution was then placed in a 1.5-ml Eppendorf tube. Each sample was incubated at 37 °C in a shaking incubator for 6 weeks at 200 rpm. Samples were removed and visualized by electron microscopy.

**Electron Microscopy (EM)**—Formvar carbon-coated copper EM grids were prepared and coated with protein samples as described previously (18). All images were taken using a CM10 electron microscope (FEI, Eindhoven, Holland) operating at 100 keV.

## RESULTS

**$\beta_2m$  Fibrillogenesis**—In order to determine whether  $\beta_2m$  forms amyloid-like fibrils in the volatile buffers required for ESI-MS analysis, the protein was incubated for 6 weeks at 0.2  $\text{mg} \cdot \text{ml}^{-1}$  in both the low salt and high salt buffers at pH 2.6 and 3.6 (see “Experimental Procedures”). After this time, an aliquot of each sample was taken and analyzed by negative stain EM. At pH 2.6, fibrils of  $\beta_2m$  had formed in both the low salt and high salt buffers (Fig. 2, *a* and *b*). In the low salt buffer (Fig. 2*a*), the fibrils were generally longer ( $\sim 5 \mu\text{m}$ ) than those formed under high salt conditions ( $\sim 1 \mu\text{m}$ ) (Fig. 2*b*). Further, in low salt buffers at pH 2.6, the majority of the fibrils observed showed distinct periodicity, whereas in high salt buffers a mixture of single protofilaments and slightly thicker fibrils with some periodicity were observed. The latter resemble type I fibrils previously identified (18) in which paired protofilaments twist around each other. At pH 3.6 (Fig. 2, *c* and *d*) the yield of fibrils was greater than at pH 2.6. In low salt buffer at pH 3.6 (Fig. 2*c*), the fibrils exhibited various degrees of lateral association. On average, these fibrils were longer than the fibrils formed at pH 2.6 in high salt buffers yet were shorter than those formed in low salt buffer at pH 2.6. At pH 3.6 under high salt conditions, a mass of aggregated material was ob-

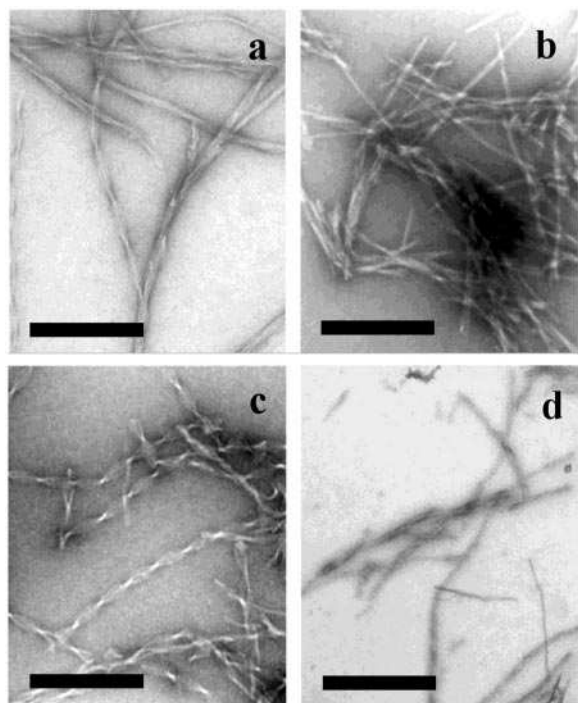


FIG. 2. **Negative stain EM images of wild-type  $\beta_2m$  fibrils.** Scale bar, 500 nm. Fibrils were formed at a protein concentration of 0.2 mg·ml<sup>-1</sup> in a shaking incubator at 37 °C (see “Experimental Procedures”). *a* and *b*, fibrils formed at pH 2.6 in low and high salt buffers, respectively. *c* and *d*, fibrils formed at pH 3.6 in low and high salt buffers, respectively. *a* and *c*, images taken after 6 weeks of incubation. *d*, image taken after 10-day incubation time.

served after 6 weeks (data not shown). However, after an incubation time of 10 days under these conditions, many short fibrils were observed (Fig. 2*d*). Thus, under the buffer conditions required for ESI-MS, *in vitro* fibrillogenesis of  $\beta_2m$  occurs, producing fibrils with morphologies that generally resemble those observed previously using nonvolatile buffers at low ionic strengths (15, 18, 19, 32).

**ESI Mass Spectra of Wild-type  $\beta_2m$  at Different pH**—Previous experiments using far UV CD have shown that acid denaturation of  $\beta_2m$  results in the formation of at least two distinct nonnative states (15). In order to quantify these states and to determine whether additional species are populated during acid denaturation of  $\beta_2m$ , ESI-MS *m/z* spectra of the protein were obtained at 21 different pH values ranging from pH 6.0 to 2.0. Selected *m/z* spectra for wild-type  $\beta_2m$  are shown in Fig. 3*a*. At pH 5.0 and above, the ESI-MS *m/z* spectra of wild-type  $\beta_2m$  are dominated by the 7+ ions. Below pH 5.0, a second envelope emerges, incorporating the 9+ to 11+ charge states. The relative intensity of the ion groups centered on the 7+ and 9+ charge states varies as the pH is reduced, to the extent that the base peak is centered on the 9+ charge state at pH ~4.0. With continued acidification, a third series of more highly charged states, which includes the 12+ to 14+ ions, is observed in the spectra. This third series has a maximal abundance at around pH 2.6 (Fig. 3*a*). Below this pH, the magnitude of this third ion abundance pattern declines with a concomitant slight increase in the peaks centered on the 9+ charge state. Presumably, this corresponds to counter ion-mediated refolding of the acid-unfolded state by the continued addition of acid to the fully charged protein (34). These data were highly reproducible. In any given experiment, a ~5% deviation from the mean value for each charge state was observed at pH 3.6 and 2.6 ( $n = 7$ , data not shown).

These data suggest that at least three different conforma-

tional states of  $\beta_2m$  are populated depending on the pH of the solution: a native state centered on the 7+ ions, a partially folded ensemble centered on or around the 9+ charge state, and a third, more expanded, acid-unfolded state emerging at higher charge states. Thus, the data agree with previous analyses using far UV CD, which suggested that partially folded  $\beta_2m$  predominates at pH 3.6, whereas more acid-unfolded conformers are preferentially stabilized at lower pH values (15).

**Linear Deconvolution of the ESI-MS Spectra of Wild-type  $\beta_2m$** —The complex, multimodal nature of the ESI-MS *m/z* spectra of wild-type  $\beta_2m$  over the pH range investigated demonstrates that the partially folded ensemble, analyzed previously at pH 3.6 (15, 21), and the acid-unfolded state, analyzed previously at pH 2.5 (22), involve the co-population of a number of distinct conformational states. Thus, at pH 3.6 the charge state distribution shows a spread of ions incorporating the 6+ to 12+ ions, suggesting co-population of the partially folded and native conformations (Fig. 3*a*). By contrast, the partially folded and acid-unfolded states are co-populated at pH 2.6. The relative proportion of each conformational state in each ensemble varies according to the pH. In order to quantify the relative contribution of each state to the total ion signal, a system of linear deconvolution was applied to each ESI-MS *m/z* spectrum over the pH range investigated (see “Experimental Procedures”).

At pH 5.0 and above, the charge state distribution of wild-type  $\beta_2m$  is described well by a single gaussian distribution representing the native state of the protein (Fig. 4). Below this pH value, however, this function does not adequately describe the data, and a second gaussian function is required to fit the charge state distribution. The second function represents the partially folded state of  $\beta_2m$  and is broader than the gaussian function of the native state, presumably arising from increased conformational heterogeneity and/or decreased structural compactness of this ensemble relative to the native protein. Between pH 4.8 and 3.8, the ESI-MS *m/z* spectra of  $\beta_2m$  can be fitted successfully to the sum of these two gaussian distributions. Further, the S.D. (population width) and mean (population central) of these distributions show little variation over this pH range (Fig. 5, *a* and *b*), whereas the amplitudes of both gaussian distributions vary, suggesting a two-state equilibrium between the native and partially folded states over this pH range (Fig. 5*c*). Below pH 3.8, the ESI-MS *m/z* spectra of wild-type  $\beta_2m$  can no longer be fitted to two gaussian distributions (Fig. 4*c*). This was highlighted by the deterioration of the fits below this pH value and by loss of continuity in the S.D. and mean of the gaussian function describing the partially folded state, which became broader and centered on higher charge states at lower pH (data not shown). These data suggest that a third conformational state is in equilibrium with native and partially folded  $\beta_2m$  below pH 3.6 and is characterized by a greater number of charges than the partially folded state. However, these data are also consistent with a two-state system where a marked increase in the structural heterogeneity of the partially folded state occurs below pH 3.8, giving rise to a broadening of the gaussian function describing this state. In either case, the data demonstrate the formation of more expanded protein conformers at lower pH values.

To reduce the residual error and also to maintain the level of global agreement between the S.D. and mean of the gaussian function corresponding to the partially folded state across the entire pH range studied, a third function was introduced within each fit. To demonstrate the requirement of a third distribution to fit the data and to quantify the contribution of this species to the equilibrium ensemble, it was assumed that the 13+ and 14+ charge states, which are not present in the ESI-MS *m/z* spectra above pH 3.4, uniquely reflect the popula-

FIG. 3. Selected ESI-MS  $m/z$  spectra of wild-type (a), V9A (b), and F30A (c) showing the variation in the charge state distributions over the pH range investigated (pH 6.0 to 2.0). All spectra were acquired on a Platform II mass spectrometer (Micromass UK/Waters) in low salt buffer acidified with concentrated HCl (see "Experimental Procedures").

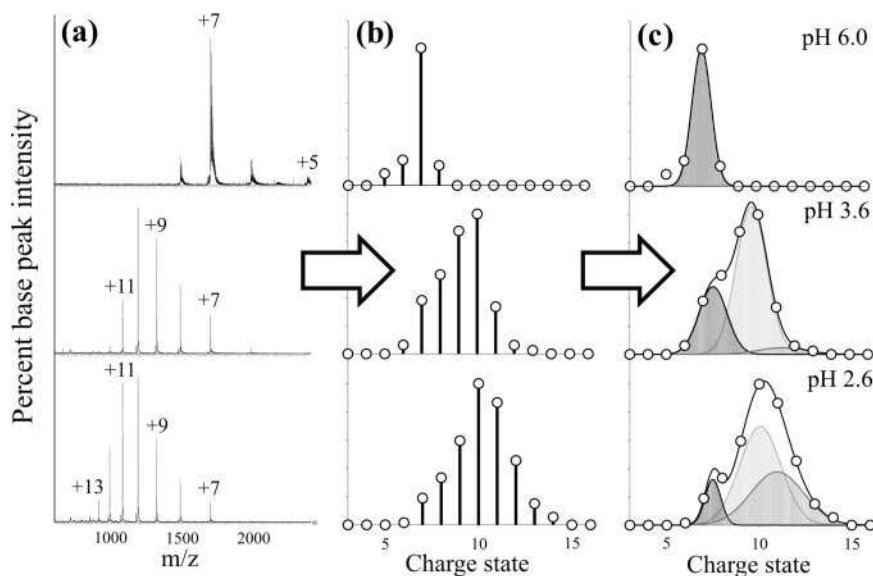
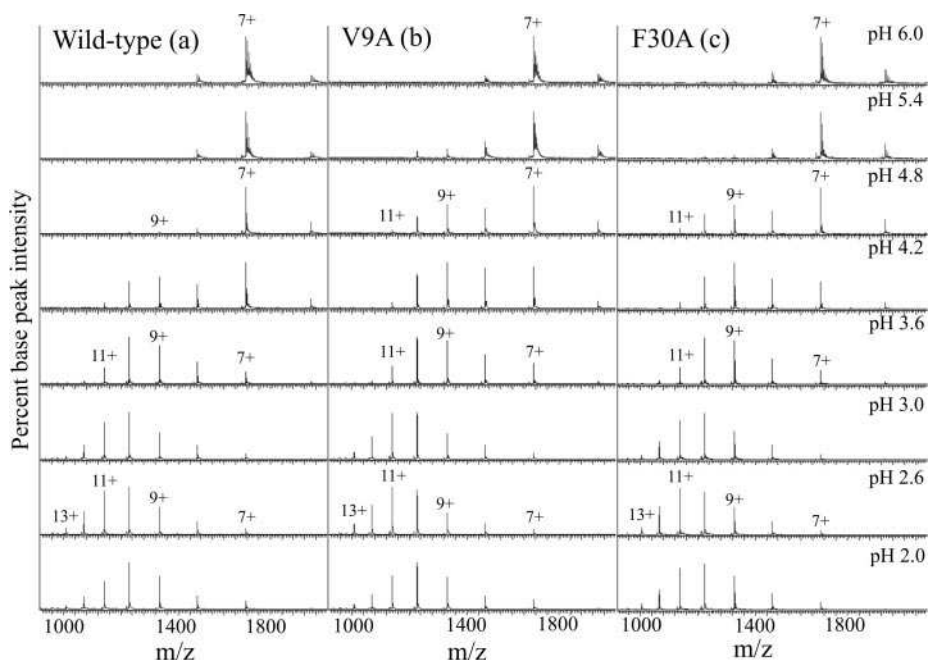


FIG. 4. Outline of the deconvolution process of ESI-MS  $m/z$  spectra of wild-type  $\beta_2m$ . Spectra were acquired on a Platform II mass spectrometer (Micromass UK/Waters) in low salt buffer acidified with concentrated HCl (see "Experimental Procedures"). a, examples shown are at pH 6.0, 3.6, and 2.6. b, spectra were transferred initially to a charge state scale where the percentage base peak intensities of all charge states were recalculated by integration of all adduct ions up to and including the dipotassium adduct ions into their respective quasimolecular ions. c, the distribution was then fitted to a limited number of gaussian functions.

tion of the acid-unfolded ensemble. By contrast, the 12+ ions contain contributions from both the partially folded and acid-unfolded states. In addition, the S.D. and the mean of the gaussian function representing the partially folded state were held constant initially with values measured at pH values where the acid-unfolded state is not populated (*i.e.* above pH 3.6). The error introduced by applying such restraints was then reduced by the inclusion of the third gaussian function representing the acid-unfolded conformation. Finally, fine tuning of any remaining error was accomplished by least squares regression using Solver (Microsoft), which was performed without any restraint of any of the parameters for all three gaussian functions (see "Experimental Procedures"). In this manner, an excellent agreement between the experimental data and the gaussian fits was obtained over the entire pH range studied.

The relative populations of the native, partially folded, and acid-unfolded states of  $\beta_2m$ , calculated from the deconvoluted ESI-MS  $m/z$  spectra across the pH range investigated, are shown in Fig. 5c. The data show that only the native protein is populated above pH 5.0. The spectra showed no evidence of a small population ( $\sim 15\%$ ) of a slowly converting nonnative spe-

cies at physiological pH previously detected by stopped flow fluorescence and capillary electrophoresis (35, 36). This could reflect differences in the buffer conditions used or would result if the partially folded and the nonnative states have similar charge state distributions. Below this pH, the native state denatures cooperatively, and the partially folded state is formed in an apparent two-state transition. At pH 3.4, the population of the partially folded state is maximal. Below pH 3.4, the partially folded state is destabilized relative to the acid-unfolded state. Thus, whereas at pH 3.4 the partially folded state predominates, the ensemble contains significant contributions from both native-like and acid-unfolded molecules ( $\sim 30$ , 65, and 5% for native, partially folded, and acid-unfolded  $\beta_2m$ , respectively) (Fig. 5c). Similarly, at pH 2.6, the equilibrium mixture contains  $\sim 10$ , 55, and 35% native, partially folded, and acid-unfolded molecules, respectively. The residual population of the charge state distributions centered on the 7+ ions at pH 2.6 is surprising. Interestingly, however, these species were lost upon reduction of the disulfide bond (data not shown), demonstrating that the disulfide bond is responsible for the survival of these compact species even un-

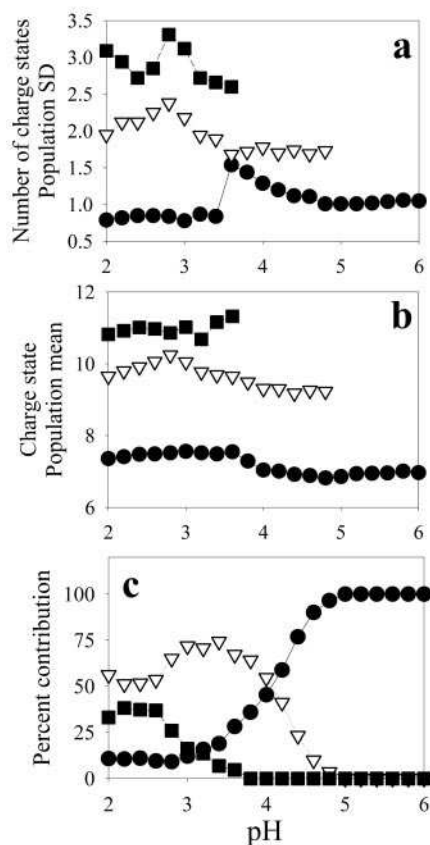


FIG. 5. Global control charts used to monitor the variation in the gaussian S.D. values (a); the gaussian mean of the native (●), partially folded (▽), and acid-unfolded (■) states of wild-type  $\beta_2m$  during acid titration (b); and percentage contribution of each state to the total ion current with varying pH (c). The conformer-specific contribution of each state shows that the denatured ensembles at pH 2.6 and 3.6 are mixtures of different conformational states. Variations in the observed mean and S.D. of the gaussian functions representative of the native, partially folded, and acid-unfolded states of  $\beta_2m$  throughout the titration result from the fitting process as each ESI-MS  $m/z$  spectrum was minimized locally at each pH value rather than globally. The average error squared of each local pH fit for wild-type  $\beta_2m$  throughout the whole titration is 1.98%.

der highly denaturing acidic conditions. Furthermore, the presence of the disulfide bond accounts for the limited resolution between the partially folded and acid-unfolded states in the ESI-MS  $m/z$  spectra of  $\beta_2m$ , since species with charge states up to 19+ were observed in the spectrum of the reduced protein at pH 2.6.

**Comparison of the Mutants V9A and F30A with Wild-type  $\beta_2m$** —To confirm the validity of the deconvolution process, the charge state distributions of two well characterized mutants of  $\beta_2m$ , V9A and F30A (20, 32), were analyzed as a function of pH using an identical procedure to that applied to the wild-type protein. Both phenylalanine 30 and valine 9 are buried in the hydrophobic core of  $\beta_2m$  (Fig. 1) (10), and their mutation disrupts the global stability of the protein. Analysis of these variants by fluorescence, near UV CD, and far UV CD has shown that both proteins have native-like structures at neutral pH but are significantly destabilized compared with wild-type  $\beta_2m$ . Thus, whereas significant denaturation (>5%) occurs below pH 4.8 for wild-type  $\beta_2m$ , this occurs at higher pH values (pH 5.6 and pH 5.3) for the V9A and F30A  $\beta_2m$  variants, respectively (20, 32).

ESI-MS  $m/z$  spectra of V9A and F30A  $\beta_2m$  as a function of pH are shown in Fig. 3, b and c. As expected from their native-like structure, the charge state distributions of both proteins

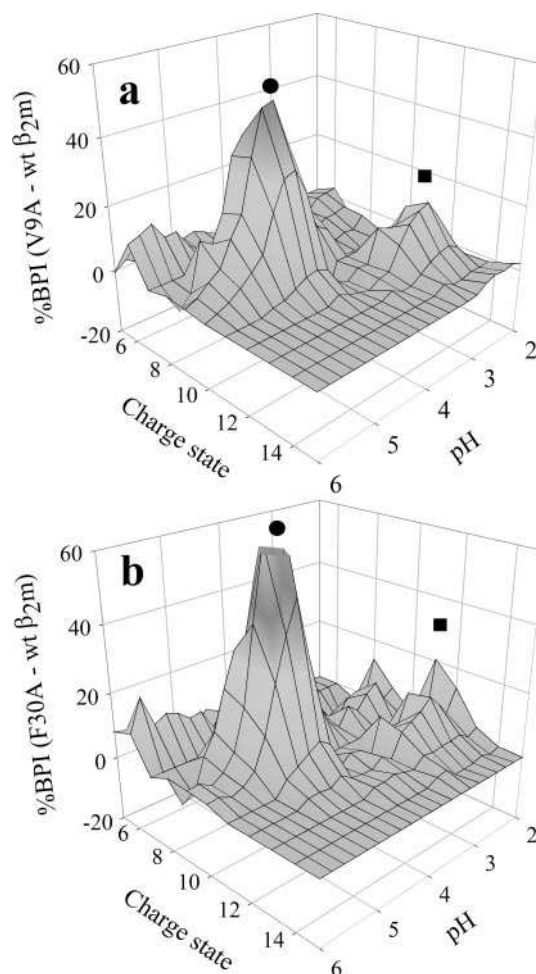


FIG. 6. Difference plots contrasting the variation in ion intensities of V9A (a) and F30A (b) with wild-type  $\beta_2m$ . The plots were drawn by subtraction of the percentage of BPI of each charge state (5+ to 15+) for wild-type  $\beta_2m$  from the corresponding spectra of the two variants. The graphs highlight two ion clusters in each mutant that differ significantly from wild-type  $\beta_2m$  centered on or around the 9+ (●) and 11+ ions (■). The higher ion charge cluster (■) is ~15% more intense for each mutant than wild-type  $\beta_2m$  below pH 3.0. The 9+ ion charge cluster (●) is significantly greater in intensity in the spectra of both variants compared with wild-type  $\beta_2m$  (~40% at pH 4.6 V9A (a) and ~60% at pH 4.8 F30A (b)).

are narrow and centered on the 7+ charge state at pH 6.0 (Fig. 3, b and c). By contrast with wild-type  $\beta_2m$ , the pH at which ions with charges of >8+ are formed significantly is higher. Thus, ions with charges of >8+ are first observed in the ESI-MS  $m/z$  spectra at pH 4.8, 5.8, and 5.4 for wild-type, V9A, and F30A  $\beta_2m$ , respectively. Furthermore, minor but significant differences in the intensities of the 12+ to 14+ ions are also observed in spectra of the mutant proteins compared with wild-type  $\beta_2m$ , particularly at pH 2.6 (Fig. 6, a and b). The results indicate that the pH of the N-I transition point measured by ESI-MS correlates closely with the results obtained previously using far UV CD (20, 32). Furthermore, the data indicate that the acid-unfolded state is more extensively populated in the variant proteins below pH 3.2, as shown by the small but significant (~15%) increase in the intensity of the 12+ to 14+ charge states for the variant proteins at this pH (Fig. 6, a and b).

Deconvolution of the ESI-MS  $m/z$  spectra of V9A and F30A  $\beta_2m$  was carried out as described above for wild-type  $\beta_2m$ . The ESI-MS  $m/z$  spectra of both variants could also be fitted to a maximum of three gaussian functions over the entire pH range studied. The percentage of conformer-specific ion signal to

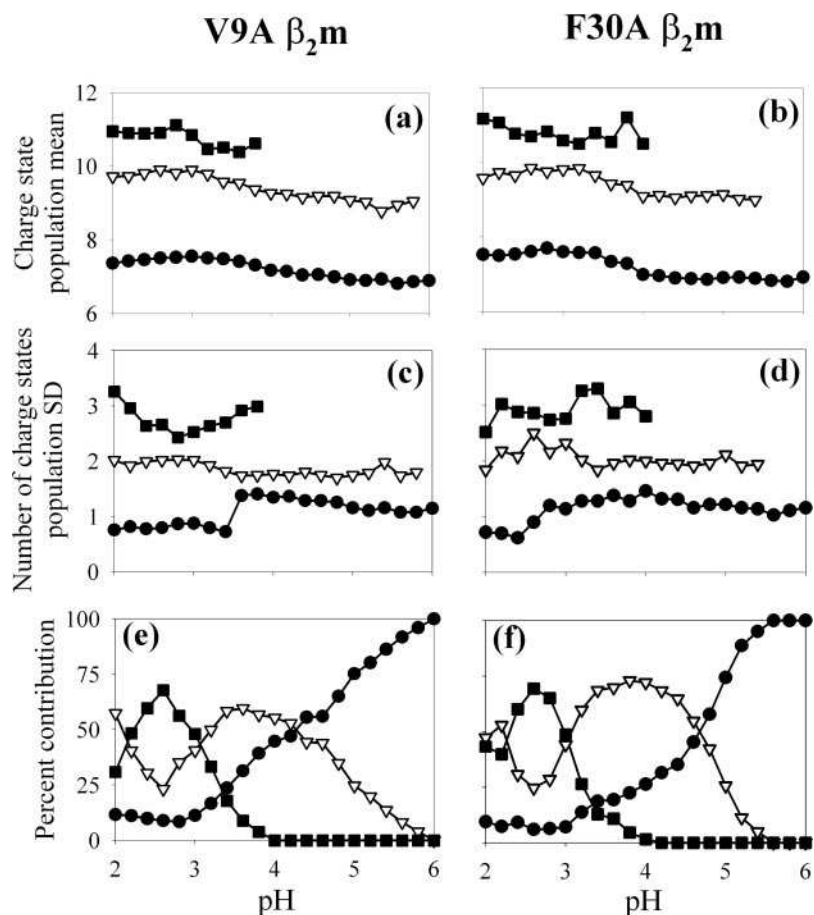


FIG. 7. Global control charts used to monitor the variation in the gaussian mean and S.D. values of the native (●), partially folded (▽), and acid-unfolded (■) states of V9A (a and c) and F30A (b and d)  $\beta_2m$  during acid titration. The percentage contribution of each state to the total ion current of both proteins at each pH is shown in e–f.

gether with the global control charts used to monitor the peak S.D. and mean of each gaussian function with varying pH is shown in Fig. 7 (a–f). The data show that the partially folded state of each variant is formed at a higher pH than observed for wild-type  $\beta_2m$ . This state is maximally populated at pH 3.6 and 3.8 for V9A and F30A, respectively, compared with pH 3.4 for wild-type  $\beta_2m$  (Figs. 5c and 7, e and f). Furthermore, the maximal population of the partially folded state at these pH values also differs significantly in the three proteins (~75% for wild-type and F30A  $\beta_2m$  compared with ~60% for V9A  $\beta_2m$ ) (Figs. 5c and 7, e and f). The acid-unfolded state is also populated significantly at pH ~3.8 for both variants and has a maximum ion contribution at pH 2.6. Interestingly, the maximal population of the acid-unfolded state also varies significantly in the three proteins (~70% for V9A and F30A compared with ~45% for wild-type  $\beta_2m$ ).

**Comparison of ESI-MS Data with Fluorescence Denaturation Curves**—The data presented above show an excellent correlation between the pH at which denaturation commences for wild-type, V9A, and F30A  $\beta_2m$  determined using ESI-MS with previous data obtained using far UV CD (20, 32). To test this correlation further, pH-induced denaturation of  $\beta_2m$  was measured using far UV CD under the low salt buffers used for the ESI-MS experiments. Significantly, analysis of the pH dependence of  $\beta_2m$  stability by far UV CD at low concentration (0.4 mg·ml<sup>-1</sup>) and in the low salt ESI-MS buffers shows that changes in signal between the partially folded and acid-unfolded states are too small to measure accurately (data not shown). By contrast, at higher protein concentrations and increased ionic strength, the CD signal monitors aggregation from rapid oligomerization of the partially folded state rather than intramolecular conformational changes under the conditions used (data not shown) (37). In order to test the results of

the ESI-MS analysis further, wild-type  $\beta_2m$  and the variant F30A were titrated with acid, and denaturation was monitored using fluorescence of the two tryptophan residues (Trp-60 and Trp-95) in each protein. In each experiment, the conditions used were identical to those employed in the ESI-MS analysis and showed no evidence for intermolecular association events. The resulting data (Fig. 8a) show that the fluorescence signal of each protein decreases with pH in a sigmoidal manner, consistent with cooperative denaturation of the proteins at acidic pH. As expected from previous results (20) and the data presented above, F30A is less stable than its wild-type counterpart, denaturation commencing at pH 5.4 for F30A compared with pH 4.8 for wild-type  $\beta_2m$  (Fig. 8a). As shown by the ESI-MS results above, acid denaturation of both F30A and wild-type  $\beta_2m$  involves a complex transition that involves at least three distinct states. To determine whether these results are consistent with the fluorescence data, the fluorescence denaturation curve of wild-type  $\beta_2m$  was computed from the known concentrations of native, partially folded and acid-unfolded states at each pH determined using ESI-MS. It was assumed that the fluorescence signals of native, partially folded, and acid-unfolded  $\beta_2m$  are distinct, and each varies linearly with pH (see “Experimental Procedures”). The resulting curve (Fig. 8b) shows a good correspondence of the computed fluorescence curve with that observed experimentally. Similarly, an excellent fit to the fluorescence denaturation curve of F30A  $\beta_2m$  was obtained using the populations determined by ESI-MS for this protein and using identical pH-dependent fluorescence values for the partially folded and acid-unfolded states (Fig. 8c). The fluorescence signal of the native states of wild-type and F30A  $\beta_2m$  and the pH dependence of these parameters were determined directly from each fluorescence denaturation curve (see “Experimental Procedures”). The fact that a good fit to the observed fluores-

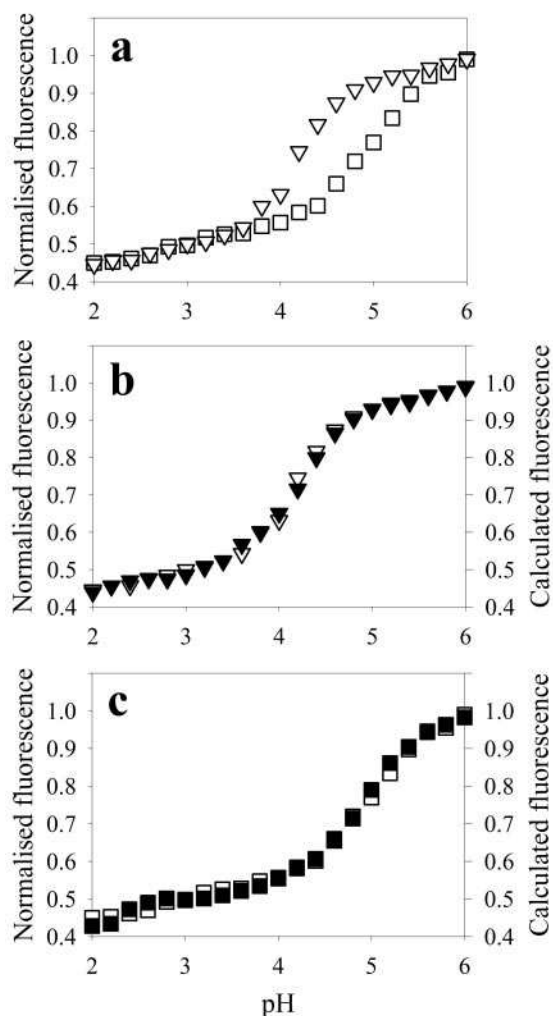


FIG. 8. *a*, equilibrium denaturation of wild-type ( $\nabla$ ) and F30A ( $\square$ )  $\beta_2m$  determined using tryptophan fluorescence. Fluorescence intensities were normalized to the signal of each protein at pH 6.2. *b* and *c*, comparison of the denaturation curves monitored by fluorescence (*open symbols*) with fluorescence curves computed from the ESI-MS-determined populations of native, partially folded, and acid-unfolded  $\beta_2m$  (*closed symbols*) for wild-type (*b*) and F30A  $\beta_2m$  (*c*), respectively.

cence data could be obtained for both proteins from the derived ESI-MS populations (squared error values of 0.003 and 0.004 for wild-type and F30A  $\beta_2m$ , respectively), using the same pH-dependent fluorescence signals for the partially folded and acid-unfolded states, further supports the validity of the deconvolution method used for the ESI-MS analysis.

#### DISCUSSION

Emerging data from ESI-MS have demonstrated the technique to be a powerful analytical tool, not simply for determining molecular masses but also in analysis of protein dynamics and the resolution of complex mixtures of different conformational species (38). Furthermore, the gentle nature of the transfer of proteins from the electrospray droplet to the gas phase means that perturbation of the solution structure of a protein is minimal (39), and there is now significant evidence to suggest that the correlation between the solution and gas phase properties of a protein is significant (27, 40, 41). An impressive and increasing number of ESI-MS-based approaches now exist with regard to the characterization of the conformational dynamics of proteins (38). Here we have demonstrated the power of ESI-MS to resolve complex mixtures of protein conformers that rely on differences in the net positive charge between native

and nonnative conformations. Such differences may originate from the diminished capacity of native proteins to stabilize charges opposite to those of the ionization mode from neutralization upon their unfolding (30), although several other models have been proposed (23, 27–29). The strength of ESI-MS, compared with other spectroscopic methods, is that each conformational ensemble of a protein can be visualized independently in the ESI  $m/z$  spectrum, provided that each state has a unique and resolved charge state distribution. Although it is feasible that conditions within the ion source during ionization and desorption could perturb the relationship between the solution and gas phase states on account of reduced pH at the capillary tip and the destabilizing effect of polyprotonation, the analysis of ESI-MS charge state distributions has been shown to be both conformationally specific (42) and insensitive to secondary solution effects (43).

Consistent with previous reports (15), our data indicate that  $\beta_2m$  populates three distinct states with varying pH. However, our results are also consistent with a two-state model in which the partially folded ensemble becomes increasingly broad with continued acidification, the partially folded and acid-unfolded states forming a continuum rather than a distinct two-state equilibrium separated by a significant free energy barrier. This is an important point, since equilibrium denaturation, monitored by fluorescence, for example, shows no evidence for a multistate system. Similarly, measurements of acid denaturation of  $\beta_2m$  using far UV CD at low concentration ( $0.4 \text{ mg}\cdot\text{ml}^{-1}$ ) and in volatile buffers also show no evidence for a multistate system. Here we interpret the emergence of the 12+ to 14+ charge states (which occurs at pH <3.8 for wild-type  $\beta_2m$ ) in terms of the population of a distinct third species of acid-unfolded molecules that are conformationally distinct relative to the partially unfolded state. In accord with this, protein conformers have been shown to have little change in their charge state distributions over wide pH ranges if their structure is known not to change over this pH range (44). In addition, NMR data suggest that by contrast with partially unfolded  $\beta_2m$ , the conformational ensemble of  $\beta_2m$  formed at pH 2.5 contains largely unfolded molecules with residual structure involving residues in the B, E, and F strands (21, 45).

Under native conditions, the V9A mutant of  $\beta_2m$  is particularly interesting in that this protein assembles spontaneously into amyloid-like fibrils with a distinct morphology (32). The ESI-MS data demonstrate that the charge state distribution of the V9A variant at pH 6.0 resembles that of wild-type  $\beta_2m$ , with no evidence for a significant population of nonnative states that exhibit distinct charge state distributions. The amyloidogenic precursors of V9A at this pH may therefore possess tertiary structures similar to that of native  $\beta_2m$  or may involve relatively minor perturbations in secondary structure, possibly involving increased local dynamics of the A-strand that are not detected by ESI-MS (32). Alternatively, the concentration of amyloidogenic states of V9A  $\beta_2m$  at pH 6.0 may simply be too low to detect by ESI-MS.

One of the most powerful aspects of analyzing the charge state distribution of a protein is its capacity to resolve and quantify different species that are co-populated in solution. In addition, the technique may be of particular importance when dealing with proteins that are prone to aggregation under certain conditions. This importance is highlighted with the  $\beta_2m$  variant V9A, since it proved impossible to acquire equilibrium denaturation curves using either far UV CD or fluorescence because of time-dependent signal changes that reflect rapid protein aggregation in the volatile buffers used. However, this phenomenon does not represent a challenge for ESI-MS, because alterations in instrumental conditions, such as the cone

voltage, can be used to disassemble solution phase aggregates (40). In addition, oligomers can be visualized in the ESI-MS  $m/z$  spectra and analyzed separately. For V9A  $\beta_2m$ , for example, minor peaks (~5% BPI) corresponding to protein dimers were visible in the ESI-MS  $m/z$  spectra above pH 4.0. However, because these peaks are resolved from those of monomers, they could be specifically excluded from the analysis of the properties of the monomeric protein.

The ESI-MS  $m/z$  spectra of wild-type  $\beta_2m$ , together with the  $\beta_2m$  mutants V9A and F30A, show transitions between the native and partially folded states that commence at pH 4.8, 5.6, and 5.4, respectively. These data are in excellent agreement with previous results obtained by far UV CD (20, 32). In addition, a close correspondence between the observed fluorescence denaturation curves and those computed from the ESI-MS-determined populations of each state is obtained. These data demonstrate the accuracy of quantification of ESI-MS  $m/z$  spectra by linear deconvolution of the charge state distributions. Moreover, the data show that even when the resolution between different charge state distributions is limited, as observed for the partially folded and acid-unfolded states of  $\beta_2m$ , ion envelopes can be assigned to different protein conformations and fitted accurately by global analysis of a series of spectra obtained using a detailed pH titration.

With regard to  $\beta_2m$  amyloidosis, our results indicate that the pH 2.6 and 3.6 ensembles are complex mixtures involving two or more distinct conformational states, consistent with line broadening seen in NMR spectra of these states (15, 21, 22). The ability to resolve the relative proportions of each conformation of  $\beta_2m$  populated under different conditions using ESI-MS should now pave the way toward the identification of the role of each species in the generation of amyloid fibrils. The data also provide the foundations for detailed investigations into the mechanism of action of potential inhibitors of  $\beta_2m$  fibrillogenesis, since even minor perturbations in the conformational equilibrium between different species can be detected and quantified.

**Acknowledgments**—We thank Dr. Alan Berry for help with MOLSCRIPT and PeakSolve software and Drs. Susan Jones and David Smith for supplying V9A and F30A  $\beta_2m$ , respectively. We are grateful to Prof. Geoff Howlett of the University of Melbourne, Robert Bateman, and Brian Green OBE of Micromass UK and all members of the Radford group for useful discussions.

## REFERENCES

- Gejyo, F., Yamada, T., Odani, S., Nakagawa, Y., Arakawa, M., Kunitomo, T., Kataoka, H., Suzuki, M., Hirasawa, Y., and Shirahama, T. (1985) *Biochem. Biophys. Res. Commun.* **129**, 701–706
- Gorevic, P. D., Casey, T. T., Stone, W. J., DiRaimondo, C. R., Prelli, F. C., and Frangione, B. (1985) *J. Clin. Invest.* **76**, 2425–2429
- Ohashi, K. (2001) *Pathol. Int.* **51**, 1–10
- Selkoe, D. J., Podlisky, M. B., Joachim, C. L., Vickers, E. A., Lee, G., Fritz, L. C., and Oltersdorf, T. (1988) *Proc. Natl. Acad. Sci. U. S. A.* **85**, 7341–7345
- Wanker, E. E. (2000) *Biol. Chem.* **381**, 937–942
- Pitkanen, P., Westermark, P., and Cornwell, G. G., III (1984) *Am. J. Pathol.* **117**, 391–399
- Dobson, C. M. (2001) *Biochem. Soc. Symp.* **68**, 1–26
- Bjorkman, P. J., Saper, M. A., Samraoui, B., Bennett, W. S., Strominger, J. L., and Wiley, D. C. (1987) *Nature* **329**, 506–512
- Hill, D. M., Kasliwal, T., Schwarz, E., Hebert, A. M., Chen, T., Gubina, E., Zhang, L., and Kozlowski, S. (2003) *J. Biol. Chem.* **278**, 5630–5638
- Saper, M. A., Bjorkman, P. J., and Wiley, D. C. (1991) *J. Mol. Biol.* **219**, 277–319
- Floege, J., Bartsch, A., Schulze, M., Shaldon, S., Koch, K. M., and Smeby, L. C. (1991) *J. Lab. Clin. Med.* **118**, 153–165
- Karlsson, F. A., Groth, T., Sege, K., Wibell, L., and Peterson, P. A. (1980) *Eur. J. Clin. Invest.* **10**, 293–300
- Mayer, G., Thum, J., Woloszczuk, W., and Graf, H. (1988) *Am. J. Nephrol.* **8**, 280–284
- Gejyo, F., Homma, N., Suzuki, Y., and Arakawa, M. (1986) *N. Engl. J. Med.* **314**, 585–586
- McParland, V. J., Kad, N. M., Kalverda, A. P., Brown, A., Kirwin-Jones, P., Hunter, M. G., Sunde, M., and Radford, S. E. (2000) *Biochemistry* **39**, 8735–8746
- Esposito, G., Michelutti, R., Verdone, G., Viglino, P., Hernandez, H., Robinson, C. V., Amoresano, A., Dal Piaz, F., Monti, M., Pucci, P., Mangione, P., Stoppini, M., Merlini, G., Ferri, G., and Bellotti, V. (2000) *Protein Sci.* **9**, 831–845
- Morgan, C. J., Gelfand, M., Atreya, C., and Miranker, A. D. (2001) *J. Mol. Biol.* **309**, 339–345
- Kad, N. M., Thomson, N. H., Smith, D. P., Smith, D. A., and Radford, S. E. (2001) *J. Mol. Biol.* **313**, 559–571
- Kad, N. M., Myers, S. L., Smith, D. P., Smith, D. A., Radford, S. E., and Thomson, N. H. (2003) *J. Mol. Biol.* **330**, 785–797
- Smith, D. P., Jones, S., Serpell, L. C., Sunde, M., and Radford, S. E. (2003) *J. Mol. Biol.* **330**, 943–954
- McParland, V. J., Kalverda, A. P., Homans, S. W., and Radford, S. E. (2002) *Nat. Struct. Biol.* **9**, 326–331
- Katou, H., Kanno, T., Hoshino, M., Hagihara, Y., Tanaka, H., Kawai, T., Hasegawa, K., Naiki, H., and Goto, Y. (2002) *Protein Sci.* **11**, 2218–2229
- Chowdhury, S. K., Katta, V., and Chait, B. T. (1990) *J. Am. Chem. Soc.* **112**, 9012–9013
- Mirza, U., Cohen, S. L., and Chait, B. T. (1993) *Anal. Chem.* **65**, 1–6
- Konermann, L., and Douglas, D. J. (1998) *Rapid Commun. Mass Spectrom.* **12**, 435–442
- Grandori, R., Matecko, I., and Muller, N. (2002) *J. Mass Spectrom.* **37**, 191–196
- Ganem, B., Li, Y. T., and Henion, J. D. (1991) *J. Am. Chem. Soc.* **113**, 7818–7819
- Felitsyn, N., Kitova, E. N., and Klassen, J. S. (2002) *J. Am. Soc. Mass Spectrom.* **13**, 1432–1442
- Cech, N. B., and Enke, C. G. (2001) *Mass Spectrom. Rev.* **20**, 362–387
- Grandori, R. (2003) *J. Mass Spectrom.* **38**, 11–15
- Fenn, J. B. (1993) *J. Am. Soc. Mass Spectrom.* **4**, 524–535
- Jones, S., Smith, D. P., and Radford, S. E. (2003) *J. Mol. Biol.* **330**, 935–941
- Dobo, A., and Kaltashov, I. A. (2001) *Anal. Chem.* **73**, 4763–4773
- Goto, Y., Calcianno, L. J., and Fink, A. L. (1990) *Proc. Natl. Acad. Sci. U. S. A.* **87**, 573–577
- Chiti, F., De Lorenzi, E., Grossi, S., Mangione, P., Giorgetti, S., Caccialanza, G., Dobson, C. M., Merlini, G., Ramponi, G., and Bellotti, V. (2001) *J. Biol. Chem.* **276**, 46714–46721
- Chiti, F., Mangione, P., Andreola, A., Giorgetti, S., Stefani, M., Dobson, C. M., Bellotti, V., and Taddei, N. (2001) *J. Mol. Biol.* **307**, 379–391
- Yamaguchi, I., Hasegawa, K., Takahashi, N., Gejyo, F., and Naiki, H. (2001) *Biochemistry* **40**, 8499–8507
- Kaltashov, I. A., and Eyles, S. J. (2002) *Mass Spectrom. Rev.* **21**, 37–71
- Fenn, J. B., Mann, M., Meng, C. K., Wong, S. F., and Whitehouse, C. M. (1989) *Science* **246**, 64–71
- Robinson, C. V., Gross, M., Eyles, S. J., Ewbank, J. J., Mayhew, M., Hartl, F. U., Dobson, C. M., and Radford, S. E. (1994) *Nature* **372**, 646–651
- Siuzdak, G., Bothner, B., Yeager, M., Brugidou, C., Fauquet, C. M., Hoey, K., and Chang, C. M. (1996) *Chem. Biol.* **3**, 45–48
- Samalikova, M., and Grandori, R. (2003) *J. Am. Chem. Soc.* **125**, 13352–13353
- Konermann, L., and Douglas, D. J. (1997) *Biochemistry* **36**, 12296–12302
- Samalikova, M., and Grandori, R. (2003) *J. Mass Spectrom.* **38**, 941–947
- Hoshino, M., Katou, H., Hagihara, Y., Hasegawa, K., Naiki, H., and Goto, Y. (2002) *Nat. Struct. Biol.* **9**, 332–336
- Khan, A. R., Baker, B. M., Ghosh, P., Biddison, W. E., and Wiley, D. C. (2000) *J. Immunol.* **164**, 6398–6405
- Kraulis, P. J. (1991) *J. Appl. Crystallogr.* **24**, 946–950